J. Math. Biol. (2014) 69:369–399
DOI 10.1007/s00285-013-0709-z

Mathematical Biology

Homogenization, sex, and differential motility predict spread of chronic wasting disease in mule deer in southern Utah

Martha J. Garlick · James A. Powell · Mevin B. Hooten · Leslie R. MacFarlane

Received: 27 December 2012 / Revised: 28 June 2013 / Published online: 12 July 2013

Abstract Chronic wasting disease (CWD) is an infectious prion disease that affects mule deer, along with other Cervids. It is a slow-developing, fatal disease which is rare in the free-ranging deer population of Utah. We present a sex-structured, spatial model for the spread of CWD over heterogeneous landscapes, incorporating both horizontal and environmental transmission pathways. To connect the local movement of deer to the regional spread of CWD, we use ecological diffusion with motility coefficients estimated from mule deer movement data. Ecological diffusion allows for aggregation of populations in desirable habitats and therefore allows for an interaction between density dependent disease transmission and landscape structure. The major innovation presented is use of homogenization to accelerate simulations of disease spread in southeastern Utah, from the La Sal Mountains near Moab to the Abajo Mountains near Monticello. The homogenized model provides accuracy while maintaining fidelity to small-scale habitat effects on deer distribution, including differential aggregation in land cover types with high residence times, with errors comparable to the order parameter measuring separation of small and large scales ($\epsilon \approx .01$ in this case). We use the averaged coefficients from the homogenized model to explore asymptotic invasion speed and the impact of current population size on disease spread in southeastern Utah.

M. J. Garlick (✉)
Mathematics and Computer Science Department, South Dakota School of Mines and Technology, Rapid City, SD 57701, USA
e-mail: martha.garlick@sdsmt.edu

J. A. Powell · M. B. Hooten
Department of Mathematics and Statistics, Utah State University, Logan, UT 84322, USA

L. R. MacFarlane
Utah Division of Wildlife Resources, Salt Lake City, UT 84114, USA

Keywords Diffusion model · Ecological diffusion · Spatial heterogeneity · Multi-scale modeling · Asymptotic speed of disease spread

Mathematics Subject Classification 35 Partial differential equations · 92 Biology and other natural sciences

1 Introduction

Chronic wasting disease (CWD) is an infectious prion disease that affects mule deer (*Odocoileus hemionus*), as well as other members of the Cervidae family, namely white-tailed deer (*Odocoileus virginianus*), elk (*Cervus elaphus*), and moose (*Alces alces shirasi*) (Baeten et al. 2007). It is a rare, slowly-developing disease that is always fatal, and infected mule deer may live 12–24 months before showing visible signs of the disease (Williams 2005). The disease may be contracted by direct contact with infected deer (Miller and Williams 2003), as well as by contact with contaminated environments (Johnson et al. 2006). Prions shed into the environment through the feces, saliva, and decaying carcasses of infected deer may remain infective for many years (Miller et al. 2004). The existence of both horizontal and environmental transmission pathways may greatly affect the spread of CWD (Almberg et al. 2011).

Miller et al. (2008) have suggested that over decades CWD may affect local population dynamics with possible long-term effects on ecosystems. Mathematical models are critical tools in assessing the impact of CWD on deer populations and analyzing different management strategies (Schauber and Woolf 2003). CWD has been modeled in many different ways, including discrete-time deterministic models (Miller et al. 2000), individual-based models (Gross and Miller 2001), difference equation models (Johns and Mehl 2006), and SI epidemic models (Miller et al. 2006; Wild et al. 2011).

Although these models have made important inroads to understanding disease dynamics, a spatial model is necessary for predicting spread of an infectious disease to new geographic regions (Smith et al. 2002), particularly considering the lingering environmental footprint of CWD. Transmission of CWD is contingent on population densities which reflect the heterogeneity of the environment, which can organize spatial processes like disease spread (Bar-David et al. 2006; Real and Biek 2007).

For the most part, spatial models for CWD have been statistical. Conner and Miller (2004) use cluster analysis and Farnsworth et al. (2006) use a Bayesian hierarchical model to study spatial spread in free-ranging mule deer populations in Colorado, while Joly et al. (2006) use spatial analysis to study the spread of CWD in white-tailed deer in Wisconsin. All of these approaches require a large body of data, which is not available in areas where the disease is in its initial stages, such as Utah.

A deterministic, process-based model does not need the same amount of data to be useful. Rates of movement can be inferred from measurements of healthy deer, and transmission parameters estimated for other populations used in an appropriately constructed mechanistic model. One mechanism to introduce spread as a spatial process involves diffusion. Diffusion was applied to epidemiology by Kendall (1965) and has been used to model the spatial spread of diseases in several wildlife populations, including rabies in fox (Kallen et al. 1985; Murray et al. 1986), foot and mouth disease in feral pigs (Pech and McIlroy 1990), and conjunctivitis in house finches (Hosseini

et al. 2006). However, these models use constant diffusion coefficients, which imply that animals move at the same rate through all habitat types. Additionally, these authors used Fickian diffusion, of the form $\frac{\partial u}{\partial t} = \nabla[D(\mathbf{x})\nabla u]$, which models the distribution of organisms from high densities to low densities at a rate proportional to the density gradient (Holmes et al. 1994). Since the diffusion equation reduces population gradients, it eventually (and unrealistically) distributes organisms across all habitats equally.

On the other hand, ecological diffusion, represented by $\frac{\partial u}{\partial t} = \nabla^2[(\mu(\mathbf{x})u]$, allows for distinct population differences at habitat boundaries (Turchin 1998; Okubo and Levin 2001; Ovaskainen 2008), reflecting the aggregation of organisms in desirable habitats and their dispersal from undesirable ones. The variable motility coefficient, $\mu(\mathbf{x})$, is inversely proportional to residence time (Turchin 1998). Population density in an area increases as motility decreases, thereby parsimoniously allowing the environment to condition disease transmission through aggregation. While it would be possible to include more complicated mechanisms for population aggregation (advective preferences or landscape source/sink terms), there is a lack of data to parameterize these terms in the case of Utah deer, as well as no need to add additional complications.

Although variable motility coefficients have been recognized as necessary to model dispersal over heterogeneous landscapes they are often abandoned in practice. This is chiefly due to the added mathematical complication and lack of data to determine motility coefficients for all landcover types in a study area. Homogenization techniques can aid in dealing with mathematical complication for numerical solutions (Garlick et al. 2011), and advances in telemetry have enhanced data collection over diverse habitats (Ostfeld et al. 2005). Homogenization is a technique for facilely accommodating small scale variability in diffusion coefficients for large scale simulation (Dewhirst and Lutscher 2009), using the method of multiple scales (Holmes 1995). 'Homogenized' partial differential equations (PDEs) are determined as solvability conditions for asymptotic expansions for PDE with rapidly-varying coefficients. To derive these solvability conditions the original problem must usually be solved on fine scales, which can be a barrier. Additionally, the technique depends on strict separation of scales between small (patch to patch, i.e. the correlation length of landcover types, generally tens of meters) and large (the distance over which patch-to-patch variability changes, generally kilometers). If the solvability criteria can be determined, the resulting homogenized equations operate on much broader scales and are orders of magnitude more efficient to solve numerically. In epidemiology homogenization has been used with Fickian diffusion to model the spread of feline leukemia (Fitzgibbon et al. 2001) and dispersal of seeds (Powell and Zimmermann 2004) and with ecological diffusion in an unstructured CWD model (Garlick et al. 2011).

In this paper we present a spatial, sex-structured model for the spread of CWD in mule deer, accounting for disease-specific behaviors of male and female deer separately through motility parameters and infection rates. Both deer-to-deer and environment-to-deer transmission are included. We apply a homogenization procedure for ecological diffusion (Garlick et al. 2011) to the system of equations to facilitate numerical solution over a large domain, simulating the spread of CWD in Southeast Utah. This homogenization procedure is strikingly simple when compared to similar techniques for Fickian diffusion equations. The homogenized system not only provides a multi-scale approach to disease spread, it also provides averaged coefficients that

can be applied to predict invasion speed and the effect of population size on disease spread, which can aid managers in decision-making.

2 Model for disease transmission and population movement

Deer behavior is dependent upon the season of the year. Female deer form matrilinear groups that show strong fidelity to winter and summer ranges. Male deer also have strong site fidelity but wander more, especially during breeding season when searching for receptive females (Nicholson et al. 1997). Males interact with each other in competition for females and males test females for receptiveness through extensive licking (Kucera 1978). Thus, male breeding behavior may contribute to higher infection rates for males (McFarlane 2007). Farnsworth et al. (2005) found CWD prevalence in males to be much higher than in females. To incorporate the behavioral differences between male and female deer, we develop a sex-structured model following the SI framework of Anderson and May (1979), with the addition of environmental hazard and ecological diffusion. Latency is not included; existence and duration of a latency period is not established (Miller et al. 2006) and evidence suggests agent shedding occurs long before clinical signs of CWD appear (Miller and Wild 2004).

The equations for susceptible deer are:

$$\frac{\partial S_F}{\partial t} = \nabla^2(\mu_F S_F) - \beta_{FF} S_F I_F - \beta_{MF} S_F I_M - \gamma_F S_F H + \Phi_F(S_F, S_M) \quad (1)$$

$$\frac{\partial S_M}{\partial t} = \nabla^2(\mu_M S_M) - \beta_{FM} S_M I_F - \beta_{MM} S_M I_M - \gamma_M S_M H + \Phi_M(S_F, S_M), \quad (2)$$

where S refers to the susceptible population density, I to the infected population density, and H to the amount of infectious material in the environment. The subscripts F and M refer to female and male deer respectively. The differential operator, ∇^2, is the Laplacian, $\frac{\partial^2}{\partial {x_1}^2} + \frac{\partial^2}{\partial {x_2}^2}$. The motility coefficients μ_F and μ_M vary over space, reflecting differences in movement patterns between males and females. We allow for an infection rate for each of four types of interactions, females infecting other females, β_{FF}, males infecting females, β_{MF}, males infecting other males, β_{MM}, and females infecting males, β_{FM}. These rates vary with season: females infect other females at a higher rate during the winter, than during the summer when they are fawning, males infect females more on winter ranges, males infect males at a higher rate during the summer and winter than during breeding season, and females infect males at a higher rate during breeding season and winter than during the summer. The parameters γ_F and γ_M are the rates at which susceptible females and males contract the disease from the environment. The functions Φ_F and Φ_M contain appropriate birth and death terms for susceptibles which are not needed in detail for our modeling approach, which will use steady-state approximations for susceptible populations.

The equations for infected deer are:

$$\frac{\partial I_F}{\partial t} = \nabla^2(\mu_F I_F) + \beta_{FF} S_F I_F + \beta_{MF} S_F I_M + \gamma_F S_F H - \omega I_F - \phi I_F \quad (3)$$

Table 1 The parameters for the CWD model and values used in the simulations

Parameter	Description	Value	Source
μ_F, μ_M	Motility coefficients	See Table 2	Estimated
$\beta_{FF}, \beta_{MF}, \beta_{FM}, \beta_{MM}$	Direct transmission rates	8.767×10^{-5} to 9.315×10^{-5} density^{-1} day^{-1}	Miller et al. (2006)
γ_F, γ_M	Transmission rates from contaminated environments	0.0022 mass^{-1} day^{-1}	Miller et al. (2006)
ω	Death rate from CWD	0.0013 day^{-1}	Miller et al. (2006)
ϕ	Cull rate	0 day^{-1}	Assigned
α_F, α_M	Rates at which prions are excreted	0.00030411 mass density^{-1} day^{-1}	Miller et al. (2006)
α_{DF}, α_{DM}	Rates at which infected carcasses pollute the environment	0.1 mass density^{-1}	Assigned
δ	Rate at which infectious material leaves the environment	0.007 day^{-1}	Miller et al. (2006)

$$\frac{\partial I_M}{\partial t} = \nabla^2(\mu_M I_M) + \beta_{FM} S_M I_F + \beta_{MM} S_M I_M + \gamma_M S_M H - \omega I_M - \phi I_M. \quad (4)$$

The death rate for infectives, ω, includes death due to CWD. It may also be influenced by the increased number of deaths of infected deer from predation (Wild et al. 2011) and vehicle collisions (Krumm et al. 2005) over that of healthy deer. In Utah visibly sick deer are euthanized and their carcasses removed. The parameter ϕ is the rate at which this culling occurs (reporting of sick deer in Utah is a rare occurrence). The total number of susceptible and infected deer is given by $N = S_F + S_M + I_F + I_M$.

The change over time of the amount of prions in the environment is modeled by a DE for environmental hazard, H,

$$\frac{\partial H}{\partial t} = \alpha_F I_F + \alpha_M I_M + \alpha_{DF}\omega I_F + \alpha_{DM}\omega I_M - \delta H. \quad (5)$$

The parameters α_F and α_M are rates that feces and urine pollute the environment, while α_{DF} and α_{DM} are rates that decaying carcasses pollute. The parameter δ is the rate at which hazardous material leaves the environment, whether via deactivation (unknown means) or being washed away or covered up by soil deposition. The parameters for this model and the subsequent simulations are given in Table 1.

2.1 Rescaling to reduce number of free parameters

In Utah the number of infected deer is much smaller than the number of susceptible deer, i.e. $0 < I_F \ll S_F, S_M$ and $0 < I_M \ll S_F, S_M$, because the disease is rare (UDWR 2012). Therefore, considering the initial density of susceptible deer to be close to the density at carrying capacity ($S_F(0) + S_M(0) = K$) and the initial density of infected deer to be much smaller ($I_F(0) + I_M(0) = \eta K, 0 < \eta \ll 1$) leads to

the following scales: $\bar{S}_F = \frac{S_F}{K}$, $\bar{S}_M = \frac{S_M}{K}$, $\bar{I}_F = \frac{I_F}{\eta K}$, $\bar{I}_M = \frac{I_M}{\eta K}$, and $\bar{H} = \frac{H}{\alpha_{DM}\eta K}$. Rescaling time with $\bar{t} = \omega t$ and assuming $\left|\nabla^2(\mu_F \bar{S}_F)\right| \sim \omega$ gives:

$$\frac{\partial \bar{S}_F}{\partial \bar{t}} = \frac{1}{\omega}\left[\nabla^2(\mu_F \bar{S}_F) + \Phi_F(\bar{S}_F) - \eta K \bar{S}_F\left(\beta_{FF}\bar{I}_F - \beta_{MF}\bar{I}_M - \gamma_F \alpha_{DM}\bar{H}\right)\right] \quad (6)$$

$$\frac{\partial \bar{S}_M}{\partial \bar{t}} = \frac{1}{\omega}\left[\nabla^2(\mu_M \bar{S}_M) + \Phi_M(\bar{S}_M) - \eta K \bar{S}_M\left(\beta_{FM}\bar{I}_F - \beta_{MM}\bar{I}_M - \gamma_M \alpha_{DM}\bar{H}\right)\right]. \quad (7)$$

Hunting and habitat management practices in Utah are aimed at reaching and maintaining a population objective for mule deer, determined by wildlife managers (UDWR 2012) and given as a number of deer. Assuming the functions Φ_F and Φ_M contain birth, death, and hunting rates such that a population level is maintained (i.e. $\frac{K\beta}{\omega} \sim 1$) and neglecting the terms multiplied by the small parameter η, (6) and (7) become:

$$\frac{\partial \bar{S}_F}{\partial \bar{t}} = \frac{1}{\omega}\nabla^2(\mu_F \bar{S}_F) \quad \text{and} \quad \frac{\partial \bar{S}_M}{\partial \bar{t}} = \frac{1}{\omega}\nabla^2(\mu_M \bar{S}_M), \quad (8)$$

which have steady state solutions $\hat{S}_F = \frac{C_F}{\mu_F}$ and $\hat{S}_M = \frac{C_M}{\mu_M}$ respectively. The constants C_F and C_M are proportional to the density at carrying capacity, K. The Utah Division of Wildlife Resources (UDWR) expresses the population of deer at carrying capacity as a target population in numbers of individuals, N. For our modeling purposes, we need that carrying capacity expressed as a density of the number of individuals per kilometer at carrying capacity, K, chosen such that $\iint_A \left(\hat{S}_F + \hat{S}_M\right) dA = KA \approx N$. Rescaling (3)–(5) and using $\hat{S}_F$ and $\hat{S}_M$ for the susceptible populations, our system becomes:

$$\frac{\partial \bar{I}_F}{\partial \bar{t}} = \frac{1}{\omega}\left[\nabla^2(\mu_F \bar{I}_F) + \left(\beta_{FF}\hat{S}_F - \omega - \phi\right)\bar{I}_F + \beta_{MF}\hat{S}_F\bar{I}_M + \gamma_F\alpha_{DM}\hat{S}_F\bar{H}\right], \quad (9)$$

$$\frac{\partial \bar{I}_M}{\partial \bar{t}} = \frac{1}{\omega}\left[\nabla^2(\mu_M \bar{I}_M) + \left(\beta_{MM}\hat{S}_M - \omega_I - \phi\right)\bar{I}_M + \beta_{FM}\hat{S}_M\bar{I}_F + + \gamma_M\alpha_{DM}\hat{S}_M\bar{H}\right], \quad (10)$$

and

$$\frac{\partial \bar{H}}{\partial \bar{t}} = \frac{\alpha_F}{\alpha_{DM}\omega}\bar{I}_F + \frac{\alpha_M}{\alpha_{DM}\omega}\bar{I}_M + \frac{\alpha_{DF}}{\alpha_{DM}}\bar{I}_F + \bar{I}_M - \frac{\delta}{\omega}\bar{H}. \quad (11)$$

Thus, the spread of CWD in the male and female populations is connected through the environmental hazard, as well as the gender-specific steady-state population sizes and infection rates. In fact, the steady-state population size of an area is inversely proportional to the motility ($\hat{S}_F \sim \frac{1}{\mu_F}$), so the density of infectives increases when the motility decreases. In other words, the environment plays a key role in how disease spreads through both density-dependent transmission and dispersal of infectives.

2.2 Homogenization

We aim to solve (9)–(11) numerically over tens of thousands of square kilometers, incorporating habitat variability resolved on a 30 m scale, employing a homogenization procedure. To illustrate this procedure, we assume that habitat structure is locally quasi-periodic, as when the landscape is composed of repetitively dispersed subpatches (Fitzgibbon et al. 2001; Garlick et al. 2011). As shown in Garlick et al. (2011), FFT analysis of landscape patterns in southern Utah indicate that quasi-periodicity is justified, and fortunately the exact landscape period (nor, indeed, quasi-periodicity itself) is not needed in order for this homogenization procedure to work. Landscape classification data is available at various resolutions. The LANDFIRE data base, from the Landscape Fire and Resource Management Planning Tools sponsored by the US Department of the Interior and the US Department of Agriculture Forest Service, classifies habitat in 30 × 30 m blocks (Department of Interior 2006). This provides the needed separation of scales, as we can regard the motilities μ_F and μ_M as varying quickly over the small scale and much more slowly over the large scale.

Let ϵ ($0 < \epsilon \ll 1$) be an order parameter representing the ratio of small and large scales (Powell and Zimmermann 2004). For example, a small scale of 30 meters and a large scale of 3 kilometers would yield $\epsilon = \frac{30}{3{,}000} = \frac{1}{100}$ (as in Garlick et al. (2011)). Let $\boldsymbol{x}$ be coordinates of the large spatial scale, with an associated slow time scale, t. Define a small scale $\boldsymbol{y}$ by $\boldsymbol{y} = \frac{\boldsymbol{x}}{\epsilon}$ and a corresponding fast time scale by $\tau = \frac{t}{\epsilon^2}$. The motility coefficients become functions of both spatial scales, $\mu_F = \mu_F(\boldsymbol{x}, \boldsymbol{y})$ and $\mu_M = \mu_M(\boldsymbol{x}, \boldsymbol{y})$. Quasi-periodicity means that there exists a vector, $\boldsymbol{p}(\boldsymbol{x})$, such that

$$\mu_F(\boldsymbol{x}, \boldsymbol{y} + \boldsymbol{p}(\boldsymbol{x})) = \mu_F(\boldsymbol{x}, \boldsymbol{y}) \quad \text{and} \quad \mu_M(\boldsymbol{x}, \boldsymbol{y} + \boldsymbol{p}(\boldsymbol{x})) = \mu_M(\boldsymbol{x}, \boldsymbol{y}), \tag{12}$$

for all $\boldsymbol{x}$ and $\boldsymbol{y}$ in the domain. Quasi-periodicity facilitates the homogenization procedure, but is not strictly necessary for it (Holmes 1995).

With the introduction of these two scales, the derivatives become: $\nabla \longrightarrow \nabla_x + \frac{1}{\epsilon}\nabla_y$, where the subscript indicates whether the long scale ($\boldsymbol{x}$) or short scale ($\boldsymbol{y}$) variable is differentiated, and $\frac{\partial}{\partial t} \longrightarrow \frac{1}{\epsilon^2}\frac{\partial}{\partial \tau} + \frac{\partial}{\partial t} = \frac{1}{\epsilon^2}\partial_\tau + \partial_t$. Substituting the new scales and derivatives into (9)–(11), after multiplication by ϵ^2, gives:

$$\begin{aligned}(\partial_\tau + \epsilon^2\partial_t) I_F = {} & \frac{1}{\omega}(\nabla_y + \epsilon\nabla_x) \cdot [(\nabla_y + \epsilon\nabla_x)\mu_F I_F] \\ & + \frac{\epsilon^2}{\omega}\left[\left(\beta_{FF}\hat{S}_F - \omega - \phi\right) I_F + \beta_{MF}\hat{S}_F I_M + \gamma_F \alpha_{DM}\hat{S}_F H\right],\end{aligned} \tag{13}$$

$$\begin{aligned}(\partial_\tau + \epsilon^2\partial_t) I_M = {} & \frac{1}{\omega}(\nabla_y + \epsilon\nabla_x) \cdot [(\nabla_y + \epsilon\nabla_x)\mu_M I_M] \\ & + \frac{\epsilon^2}{\omega}\left[\left(\beta_{MM}\hat{S}_M - \omega - \phi\right) I_M + \beta_{FM}\hat{S}_M I_F + \gamma_M \alpha_{DM}\hat{S}_M H\right],\end{aligned} \tag{14}$$

and

$$(\partial_\tau + \epsilon^2 \partial_t) H = \epsilon^2 \left[\frac{\alpha_F + \alpha_{DF}\omega}{\alpha_{DM}\omega} I_F + \left(\frac{\alpha_M}{\alpha_{DM}\omega} + 1 \right) I_M - \frac{\delta}{\omega} H \right], \tag{15}$$

where we have dropped the bar notation on the rescaled variables for convenience.

We replace I_F with a series expansion in ϵ:

$$I_F = I_{F_0} + \epsilon I_{F_1} + \epsilon^2 I_{F_2} + O(\epsilon^3), \tag{16}$$

and use similar expansions for I_M and H. Collecting terms at common powers of ϵ, the $O(1)$ equations are:

$$\partial_\tau I_{F_0} = \frac{1}{\omega} \nabla_y^2 (\mu_F I_{F_0}), \tag{17}$$

$$\partial_\tau I_{M_0} = \frac{1}{\omega} \nabla_y^2 (\mu_M I_{M_0}), \tag{18}$$

and

$$\partial_\tau H_0 = 0. \tag{19}$$

Since (17) and (18) are parabolic, the solutions decay exponentially to their steady state in fast time scales (Garlick et al. 2011). The steady-state solutions for I_{F_0} and I_{M_0} are:

$$I_{F_0} = \frac{c_{IF}(\boldsymbol{x}, t)}{\mu_F(\boldsymbol{x}, \boldsymbol{y})} \quad \text{and} \quad I_{M_0} = \frac{c_{IM}(\boldsymbol{x}, t)}{\mu_M(\boldsymbol{x}, \boldsymbol{y})}, \tag{20}$$

where c_{IF} and c_{IM} are functions without any $\boldsymbol{y}$ or τ dependence. The leading order solution for environmental hazard, $H_0 = H_0(\boldsymbol{x}, \boldsymbol{y}, t)$, however, depends on both spatial scales.

The $O(\epsilon)$ equations are:

$$\partial_\tau I_{F_1} = \frac{1}{\omega} \left[\nabla_y^2 (\mu_F I_{F_1}) + \nabla_y \cdot \left[\nabla_x \left(\mu_F I_{F_0} \right) \right] + \nabla_x \cdot \left[\nabla_y \left(\mu_F I_{F_0} \right) \right] \right], \tag{21}$$

$$\partial_\tau I_{M_1} = \frac{1}{\omega} \left[\nabla_y^2 (\mu_M I_{M_1}) + \nabla_y \cdot \left[\nabla_x \left(\mu_M I_{M_0} \right) \right] + \nabla_x \cdot \left[\nabla_y \left(\mu_M I_{M_0} \right) \right] \right], \tag{22}$$

and

$$\partial_\tau H_1 = 0. \tag{23}$$

Substituting (20) into (21) and (22) and simplifying (noting that $\nabla_y (\mu_F I_{F_0}) = \nabla_y c_{IF}(\boldsymbol{x}, t) = 0$ and $\nabla_y (\mu_M I_{M_0}) = \nabla_y c_{IM}(\boldsymbol{x}, t) = 0$), we obtain

$$\partial_\tau I_{F_1} = \nabla_y^2 (\mu_F I_{F_I}) \quad \text{and} \quad \partial_\tau I_{M_1} = \nabla_y^2 (\mu_M I_{M_I}). \tag{24}$$

Considering the steady state problems for I_{F_1} and I_{M_1} as in the $O(1)$ case and solving (23), yields solutions:

$$I_{F_1} = \frac{b_{IF}(\boldsymbol{x}, t)}{\mu_F(\boldsymbol{x}, \boldsymbol{y})}, \quad I_{M_1} = \frac{b_{IM}(\boldsymbol{x}, t)}{\mu_M(\boldsymbol{x}, \boldsymbol{y})}, \quad \text{and} \quad H_1 = b_H(\boldsymbol{x}, \boldsymbol{y}, t). \tag{25}$$

The solutions in (25) are precisely the same form as the solutions in (20), therefore any boundary condition satisfied by (20) leaves homogeneous boundary conditions for (25), giving $I_{F_1} = I_{M_1} = H_1 = 0$.

The $O(\epsilon^2)$ equations are:

$$\begin{aligned}\partial_\tau I_{F_2} + \partial_t I_{F_0} = \frac{1}{\omega}\Big[&\nabla_y^2(\mu_F I_{F_2}) + \nabla_x^2(\mu_F I_{F_0}) + \gamma_F \alpha_{DM} \hat{S}_F H_0 \\ &+ \left(\beta_{FF}\hat{S}_F - \omega - \phi\right) I_{F_0} + \beta_{MF}\hat{S}_F I_{M_0}\Big],\end{aligned} \tag{26}$$

$$\begin{aligned}\partial_\tau I_{M_2} + \partial_t I_{M_0} = \frac{1}{\omega}\Big[&\nabla_y^2(\mu_M I_{M_2}) + \nabla_x^2(\mu_M I_{M_0}) + \gamma_M \alpha_{DM} \hat{S}_M H_0 \\ &+ \left(\beta_{MM}\hat{S}_M - \omega - \phi\right) I_{M_0} + \beta_{FM}\hat{S}_M I_{F_0}\Big],\end{aligned} \tag{27}$$

and

$$\partial_\tau H_2 + \partial_t H_0 = \frac{\alpha_F}{\alpha_{DM}\omega} I_{F_0} + \frac{\alpha_M}{\alpha_{DM}\omega} I_{M_0} + \frac{\alpha_{DF}}{\alpha_{DM}} I_{F_0} + I_{M_0} - \frac{\delta}{\omega} H_0, \tag{28}$$

where the mixed derivative terms containing I_{F_1} or I_{M_1} have vanished since $I_{F_1} = I_{M_1} = 0$.

In the fast time scale, τ, I_{F_2} and I_{M_2} tend to steady state solutions rapidly, so relevant equations in the slower time scale are

$$\begin{aligned}\partial_t \frac{c_{IF}}{\mu_F} = \frac{1}{\omega}\Big[&\nabla_y^2(\mu_F I_{F_2}) + \nabla_x^2 c_{IF} + \gamma_F \alpha_{DM} \hat{S}_F H_0 \\ &+ \left(\beta_{FF}\hat{S}_F - \omega - \phi\right) \frac{c_{IF}}{\mu_F} + \beta_{MF}\hat{S}_F \frac{c_{IM}}{\mu_M}\Big],\end{aligned} \tag{29}$$

$$\begin{aligned}\partial_t \frac{c_{IM}}{\mu_M} = \frac{1}{\omega}\Big[&\nabla_y^2(\mu_M I_{M_2}) + \nabla_x^2 c_{IM} + \gamma_M \alpha_{DM} \hat{S}_M H_0 \\ &+ \left(\beta_{MM}\hat{S}_M - \omega - \phi\right) \frac{c_{IM}}{\mu_M} + \beta_{FM}\hat{S}_M \frac{c_{IF}}{\mu_F}\Big],\end{aligned} \tag{30}$$

and

$$\partial_t H_0 = \frac{\alpha_F}{\alpha_{DM}\omega}\frac{c_{IF}}{\mu_F} + \frac{\alpha_M}{\alpha_{DM}\omega}\frac{c_{IM}}{\mu_M} + \frac{\alpha_{DF}}{\alpha_{DM}}\frac{c_{IF}}{\mu_F} + \frac{c_{IM}}{\mu_M} - \frac{\delta}{\omega} H_0, \tag{31}$$

where the values for I_{F_0} and I_{M_0} in (20) have been used to write equations in terms of dependent variables on slower scales, $c_{IF}(\boldsymbol{x}, t)$ and $c_{IM}(\boldsymbol{x}, t)$. Note that dependence on the small scale, $\boldsymbol{y}$, is retained through coefficients containing $\hat{S}_F$ or $\hat{S}_M$.

We now explain the averaging procedure associated with homogenization in two spatial dimensions in terms of infected females. The procedure is the same for infected males. Let $\boldsymbol{p}(\boldsymbol{x})$ in (12) be defined as the periodicity vector $\boldsymbol{p}(\boldsymbol{x}) = [l_1(x_1), l_2(x_2)]^T$.

We determine the homogenized problem by averaging each term of the system (29)–(31) over a $l_1(x_1) \times l_2(x_2)$ cell, with area $A_{\text{cell}} = l_1(x_1)l_2(x_2)$. The average of a function $v(\boldsymbol{x}, \boldsymbol{y})$ over an $l_1(x_1) \times l_2(x_2)$ cell is defined as

$$\langle v \rangle = \frac{1}{A_{\text{cell}}} \int_0^{l_1(x_1)} \int_0^{l_2(x_2)} v(\boldsymbol{x}, \boldsymbol{y}) dy_1 dy_2, \tag{32}$$

a local average for the current position of interest (Holmes 1995).

Using periodicity on a cell and the Divergence Theorem,

$$\left\langle \nabla_y{}^2(\mu_F I_{F_2}) \right\rangle = \frac{1}{A_{\text{cell}}} \int_{\partial\Omega_0} \boldsymbol{n} \cdot \nabla_y(\mu_F I_{F_2}) dS_y = 0, \tag{33}$$

where $\partial\Omega_0$ is the boundary of the cell, $\boldsymbol{n}$ is the outward normal vector, and dS_y is along the cell boundary. The periodicity on the small scale also gives that the flux of individuals on either side of the cell boundary is the same. The number of infected individuals that are mobile (i.e. leaving the area) is proportional to $\mu_F I_F$, and continuity conditions therefore apply to this quantity, i.e., $\mu_F I_F$ (the number of individuals) and $\nabla(\mu_{F_1} I_F)$ (the flux) are continuous across boundaries. The net flux of individuals over the boundary is proportional to the first derivative of $\mu_F I_F$ (as opposed to μ_F times the derivative of I_F), which is a consequence of the ecological diffusion model for movement. Similarly, $\langle \nabla_y^2(\mu_M I_{M_2}) \rangle = 0$.

We apply averaging to all terms in (29). This means the parameters that depend on small-scale variability $\boldsymbol{y}$ stay inside of averages of the form (32), while parameters and variables without $\boldsymbol{y}$ dependence can be moved outside of the averages, i.e.,

$$\left\langle \partial_t \frac{c_{IF}}{\mu_F} \right\rangle = \left\langle \frac{1}{\mu_F} \right\rangle \partial_t c_{IF}, \tag{34}$$

$$\left\langle \nabla_x^2 c_{IF} \right\rangle = \nabla_x^2 c_{IF}, \tag{35}$$

$$\left\langle \frac{1}{\omega} \left(\beta_{FF} \hat{S}_F - \omega - \phi \right) \frac{c_{IF}}{\mu_F} \right\rangle = \left\langle \frac{1}{\omega} \left(\beta_{FF} \hat{S}_F - \omega - \phi \right) \frac{1}{\mu_F} \right\rangle c_{IF}, \tag{36}$$

$$\left\langle \frac{\beta_{MF} \hat{S}_F}{\omega} \frac{c_{IM}}{\mu_M} \right\rangle = \frac{\beta_{MF}}{\omega} \left\langle \frac{\hat{S}_F}{\mu_M} \right\rangle c_{IM}, \tag{37}$$

and

$$\left\langle \frac{\gamma_F \alpha_{DM} \hat{S}_F}{\omega} H_0 \right\rangle = \frac{\gamma_F \alpha_{DM}}{\omega} \left\langle \hat{S}_F H_0 \right\rangle. \tag{38}$$

The averages are similar for the equation for I_M and H_0, except that the environmental hazard H_0 depends upon both spatial scales, so it must remain inside of the averages.

We obtain our homogenized system after averaging (29)–(31) and simplifying. The homogenized equations are differential equations in the large spatial and slow time scales, with small-scale variability expressed through the averages:

$$\begin{aligned}\partial_t c_{IF} &= \frac{\bar{\mu}_F}{\omega}\nabla_x^2 c_{IF} + \bar{\mu}_F\left\langle \frac{1}{\omega}\left(\beta_{FF}\hat{S}_F - \omega - \phi\right)\frac{1}{\mu_F}\right\rangle c_{IF} \\ &\quad + \bar{\mu}_F\frac{\beta_{MF}}{\omega}\left\langle\frac{\hat{S}_F}{\mu_M}\right\rangle c_{IM} + \bar{\mu}_F\frac{\gamma_F\alpha_{DM}}{\omega}\left\langle \hat{S}_F H_0\right\rangle, \qquad (39)\\ \partial_t c_{IM} &= \frac{\bar{\mu}_M}{\omega}\nabla_x^2 c_{IM} + \bar{\mu}_M\left\langle \frac{1}{\omega}\left(\beta_{MM}\hat{S}_M - \omega - \phi\right)\frac{1}{\mu_M}\right\rangle c_{IM} \\ &\quad + \bar{\mu}_M\frac{\beta_{FM}}{\omega}\left\langle\frac{\hat{S}_M}{\mu_F}\right\rangle c_{IF} + \bar{\mu}_M\frac{\gamma_M\alpha_{DM}}{\omega}\left\langle \hat{S}_M H_0\right\rangle, \qquad (40)\end{aligned}$$

and

$$\partial_t\langle H_0\rangle = \bar{\mu}_F^{-1}\left(\frac{\alpha_F}{\alpha_{DM}\omega} + \frac{\alpha_{DF}}{\alpha_{DM}}\right)c_{IF} + \bar{\mu}_M^{-1}\left(\frac{\alpha_M}{\alpha_{DM}\omega} + 1\right)c_{IM} - \frac{\delta}{\omega}\langle H_0\rangle, \qquad (41)$$

where $\bar{\mu}_F = \frac{1}{\left\langle\frac{1}{\mu_F}\right\rangle}$ and $\bar{\mu}_M = \frac{1}{\left\langle\frac{1}{\mu_M}\right\rangle}$. In fact, $\bar{\mu}_F$ and $\bar{\mu}_M$ are harmonic averages of the motilities, a natural product of this form of homogenization (Garlick et al. 2011).

Note that (41) is in terms of the averaged environmental hazard, $\langle H_0\rangle$, the hazard terms in (39) and (40) are averages of steady state populations multiplying the hazard, $\left\langle\hat{S}_F H_0\right\rangle = C_F\left\langle\frac{H_0}{\mu_F}\right\rangle$ and $\left\langle\hat{S}_M H_0\right\rangle = C_M\left\langle\frac{H_0}{\mu_M}\right\rangle$. It is a reasonable assumption that there is a correlation between the deer aggregation and prion contamination. Therefore, in the following simulations, we used $\left\langle\frac{H_0}{\mu_F}\right\rangle = \sigma_F\left\langle\frac{1}{\mu_F}\right\rangle\langle H_0\rangle$ and $\left\langle\frac{H_0}{\mu_M}\right\rangle = \sigma_M\left\langle\frac{1}{\mu_M}\right\rangle\langle H_0\rangle$ for constants σ_F and σ_M. The constants can be calculated by returning to the small scale to compute the difference between $\left\langle\frac{H_0}{\mu_F}\right\rangle$ and $\left\langle\frac{1}{\mu_F}\right\rangle\langle H_0\rangle$ after each time step. This is a time consuming process and we found that over a sufficient time period ($\geq$1 year), $\sigma_F = \sigma_M = 1$ gives very similar results, as shown in the next section.

Our homogenized model is much easier to solve numerically than (9)–(11), yet retains the small scale variability through division by the motility coefficient (20). This allows us to run simulations over a large domain, exploring several different spread scenarios.

3 Simulating spread of CWD

CWD was first detected in the free-ranging mule deer population in the La Sal Mountains of Utah in 2002. Since then 54 positive cases have been identified in the state out of 19,000 deer tested. The area with the highest prevalence is the La Sal

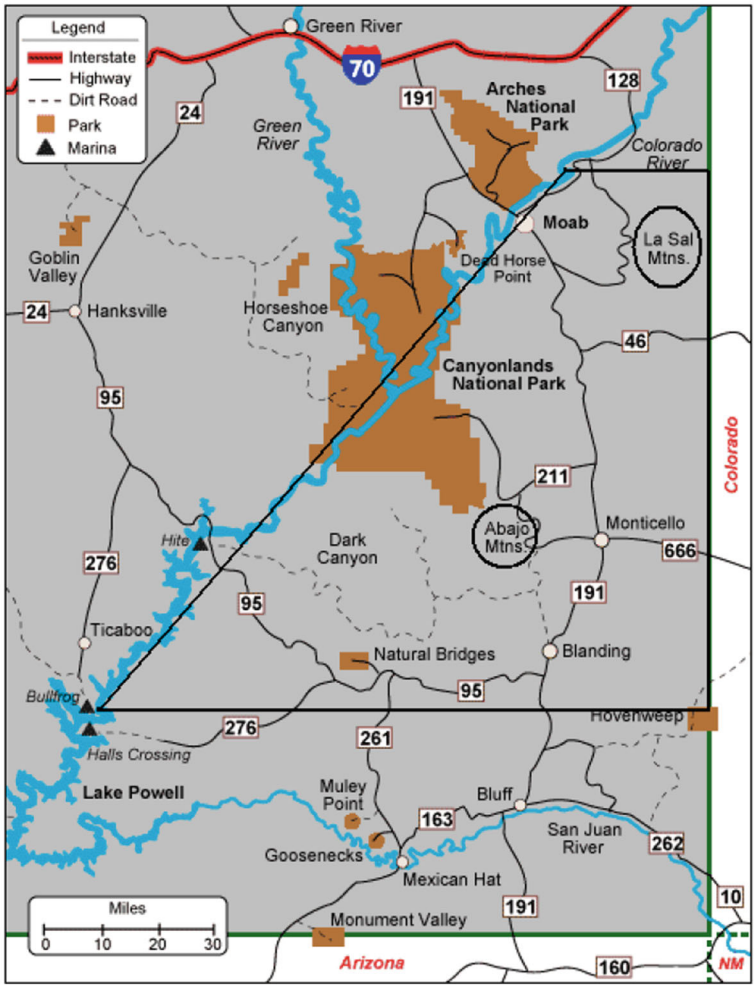

Fig. 1 A map of Southeast Utah which includes the La Sal Mountains and the Abajo Mountains (*circled*) (Rasmussen 2012). Our study area is enclosed by the *trapezoid*. The Colorado River acts as a barrier to deer movement

Mountains in Southeast Utah with 38 of the positive cases (UDWR 2012). During the 2011 hunting season the first positive CWD case was found in the vicinity of the Abajo Mountains. Exploring the spread of CWD from the La Sal Mountains southwest to the Abajo Mountains is the objective for our simulations. A map of Southeast Utah with these mountain ranges circled is found in Fig. 1. In this section, we define the area for the simulations, including boundary and initial conditions. We explain our method for estimating motilities from GPS collar data and outline sources for the other model parameters. Then we describe the assumptions for the different simulations and compare the results.

3.1 Study area

Our study area is the trapezoidal region east of the Colorado River in Southeast Utah (Fig. 1). The Colorado River acts as a barrier to deer movement (Hanks et al. 2010), so we approximate it by a line and reflect motility and population variables across it to create a no-flux boundary (see Fig. 2). No-flux boundary conditions are used for the other boundaries of the region as well, assuming no deer enter or leave.

Characteristic of the Colorado Plateau ecoregion (Watkins et al. 2007), our study area is comprised of high altitude subalpine forest (the La Sal and Abajo mountains) surrounded by valleys, canyons, shrubland, deserts, and farmland. Most deer migrate, sometimes for more than 80 kilometers, between lower elevation winter ranges and higher elevation summer ranges. Important winter range habitats include sagebrush-steppe, pinyon-juniper woodlands, salt desert shrub, and ponderosa pine forests below 7,500 feet. Summer habitats include aspen forests, mountain shrub communities, Gambel oak forests, montane sagebrush-steppe, spruce-fir and mixed conifer forests, montane parks and meadows, and agricultural areas (Plummer et al. 1968).

Since the La Sal and Abajo mountains are approximately 100 kilometers apart (see Fig. 1), separated by critical winter range habitat, a management concern has been the spread of CWD from the La Sals to the Abajos. The first CWD positive deer was found near the Abajos during the 2011 hunting season and it is of some management concern whether this spread is a fluke or whether we can expect the spread to continue and the disease establish in novel territory. The study area including these two mountain ranges is chosen so that we can explore these questions.

The Utah Division of Wildlife Resources (UDWR) divides the state into Wildlife Management Units. Our study area is contained in two of those units, La Sal (#13) and San Juan (#14). A 15 buck/100 doe ratio is a population management goal in these units. Steady-state populations for our simulations were based on post-hunting season population estimates of the UDWR (UDWR 2012). The UDWR estimates a 2 % CWD prevalence in bucks in the La Sal Mountains, while prevalence is believed to be less than 1 % in the doe population (UDWR 2012). Samples are collected from hunter-harvested male deer for testing, since female deer are not routinely hunted in Utah, resulting in a lack knowledge about CWD prevalence in females.

3.2 Model parameters

In 2005–2006, the UDWR collared 50 deer, a mix of adult males, young males, and adult females, in the La Sal Mountains. GPS data was collected on their movement, with an emphasis on deer locations during breeding season, to explore the connection between breeding behaviors and movement (McFarlane 2007). The time intervals for collecting location data depended on the time of year: 12 h intervals in late winter/early spring, 6 h intervals during spring migration/early summer, 12 h intervals during summer/early fall, and 30 min intervals during fall migration/breeding season.

Mule deer exhibit high site fidelity to traditional summer and winter ranges with seasonal migration occurring during specific times of the year. Females form matrilinear groups which remain cohesive, particularly during the breeding season when males

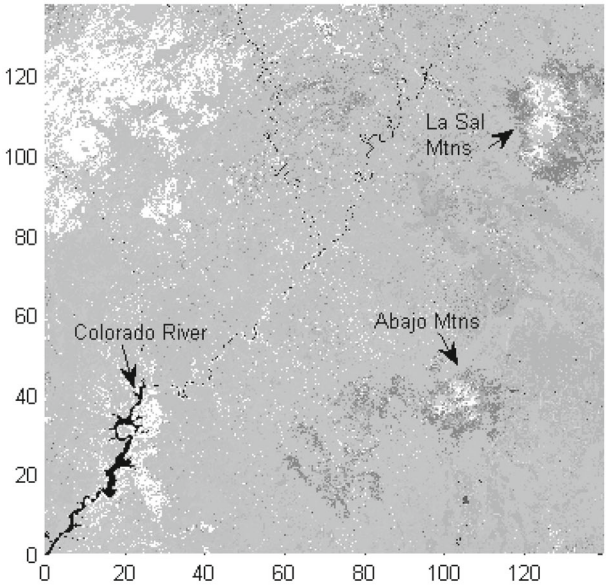

(a) Breeding season motilities for male deer

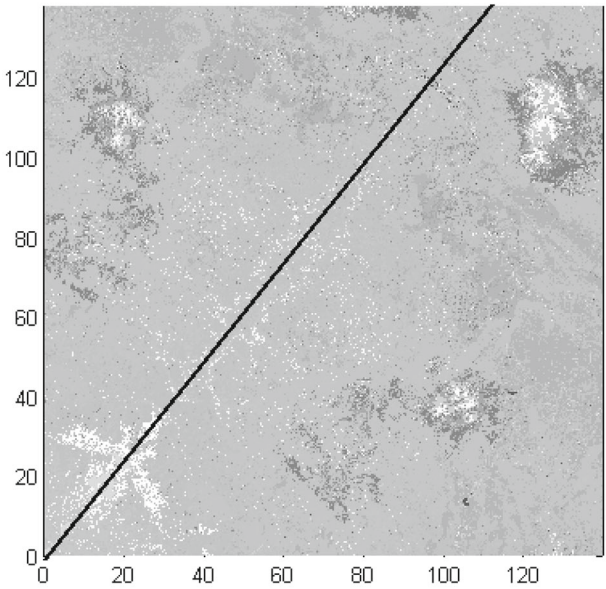

(b) Reflection about the Colorado River

Fig. 2 Motilities for male deer during breeding season. *Dark shades* indicate small motility values, while *light shades* indicate large values. The area for our simulation is the trapezoidal region east of the Colorado River shown in **a**. The Colorado River is approximated by a *line* and values are reflected across that *line*, to create no-flux condition at the boundary, as shown in **b**

begin wandering between groups looking for receptive females (McFarlane 2007). This somewhat complicates the idea of a motility being assigned to a land cover type, because the use of various habitats by deer varies widely by sex and season. Partitioning the GPS movement data by sex and by season allowed us to estimate motilities for males and females during winter, summer, and breeding season. We did not compute motilities specifically for spring or fall migration, since migration occurs during a relatively short period of time and represents the change of motility between seasons, i.e. we treat spring migration as the transient population response to the change in motilities between winter and summer.

To obtain motility coefficients, we used movement data from 11 female deer and 11 male deer, selected for having the most complete data (approximately a year long). We need motility coefficients (inverse residence times) on 30 m habitat patches appearing in southern Utah; unfortunately the GPS returns from these 22 deer are pretty sparse across habitat types (particularly in patches where deer spend little time, which would most strongly influence spread rates). Fortunately, the problem of estimating residence times using sporadic GPS data has already been addressed (Johnson et al. 2008). Johnson et al. used a continuous time correlated random walk model (CTCRW) to construct posterior distributions of most likely paths between GPS measurements. This allowed them to estimate residence times for habitats between sample points, conditioned on the distribution of possible paths.

We used the R contributed package CRAWL were used to fit Johnson et al.'s CTCRW model to our deer location data and drew 50 samples of possible paths between subsequent GPS observations to build distributions of locations at 1 min time intervals, as outlined in Garlick (2012) and briefly described here. If $\boldsymbol{m}(t)$ is a continuous, smooth path of locations, then the instantaneous rate of change in location is velocity, $\boldsymbol{v}(t)$. An Ornstien–Uhlenbeck process can be used to model velocity, defined by

$$\boldsymbol{v}(t+\Delta) = \boldsymbol{\gamma} + e^{-\beta\Delta}[\boldsymbol{v}(t) - \boldsymbol{\gamma}] + \boldsymbol{\zeta}(\Delta), \tag{42}$$

where Δ is the change in time, $\boldsymbol{\gamma}$ is mean velocity, β is an autocorrelation parameter, and $\boldsymbol{\zeta}$ is a two-dimensional Gaussian random variable,

$$\boldsymbol{\zeta} \sim N(0, \sigma^2[1 - \exp(-2\beta\Delta)]/2\beta). \tag{43}$$

The correlation parameter, β, controls how rapidly the influence of past speed decays; large β implies more rapid decay. The parameter σ controls the overall variability in velocity through the time step Δ. When Δ is close to zero there is almost no change in velocity. However, when $\Delta \to \infty$ the next velocity is completely random with variance σ^2. Equations (42) and (43) are therefore defining the velocity at time $t + \Delta$ as a random variable whose variance grows with Δ plus an adjustment related to the velocity at time t. Then $\boldsymbol{m}(t)$ is a continuous-time location process obtained by

$$\boldsymbol{m}(t) = \boldsymbol{m}(0) + \int_0^t \boldsymbol{v}(s)ds. \tag{44}$$

Thus a model for animal location is obtained by modeling velocity. The CTCRW model is defined by (42) and (44).

A sample of 50 possible paths were drawn from the predictive posterior distribution for possible paths for each deer. We used the LANDFIRE data set (Department of Interior 2006) to classify each predicted location by land cover type. Minutes spent in each of 38 land cover types were counted and the mean time spent (residence times) calculated in units of minutes per block. The small-scale motility coefficients were obtained from the residence times by taking the multiplicative inverse and converting to units of square kilometers per day. Even with 50 samples, some classifications did not contain any data points or predicted locations during a particular season; these were assigned motilities of 12.96 (residence time of only a second) to avoid division by zero. This value is sufficiently high to keep deer densities extremely low in those areas during the simulations. The motility coefficients are found in Table 2. The summer, breeding season, and winter motilities for male and female deer are compared in Fig. 3 for the area containing the La Sal Mountains.

The other parameters used in the simulations are found in Table 1, many from Miller et al. (2006). Since Miller et al. fit their ordinary differential equation models with data from captive mule deer, they adjusted the infection rate downward by a factor of ten for free-ranging mule deer, assuming that natural populations would exhibit one tenth the density. Our model uses motilities to reflect the spatial spread of the disease, which means that where motility is low, the deer are congregating, occasionally as tightly as the captive herd in Miller et al. (2006). It is therefore unclear what infectivity parameters to use. We explore infection rates between the scaled and unscaled values in the simulations.

Our model assumes a steady-state population in the study area. This means that even though the seasonal change in motilities redistributes the deer at the beginning of each season, the total number of deer, N, in the domain needs to remain the same. The constants, C_F and C_M for the steady-state population densities, $\hat{S}_F = \frac{C_F}{\mu_F}$ and $\hat{S}_M = \frac{C_M}{\mu_M}$, were computed separately for each season to maintain an appropriate number of susceptible deer but redistribute the corresponding population densities according to seasonal motilities.

3.3 Simulations

We conducted several simulations of the spread of CWD from the La Sal Mountains to the Abajo Mountains, exploring different infection rates. The use of variable motility was compared to a constant motility and the model with environment hazard was compared to one without. Other simulations explored the spread during different seasons and a comparison of two ways to average the environmental hazard, $\left\langle \frac{H_0}{\mu_F} \right\rangle$ (the average that is the consequence of homogenization) or $\left\langle \frac{1}{\mu_F} \right\rangle \langle H_0 \rangle$ (an approximation based on the assumption that deer aggregation and prion contamination are correlated), as discussed at the end of Sect. 2.2.

An alternating direction implicit (Mitchell and Griffiths 1980) numerical method was adapted for the system of homogenized equations (39)–(41) (see Garlick 2012).

Table 2 Mule deer motility coefficients in square kilometers per day

LANDFIRE	Winter		Summer		Breeding	
Classification, EVT	Male	Female	Male	Female	Male	Female
11 Open water (0.14 %)	0.10	0.22	0.29	0.40	0.27	0.99
21 Dev. open space (0.11 %)	0.57	0.44	0.16	0.12	0.25	0.05
22 Dev. low intensity (0.11 %)	0.54	0.38	0.07	0.08	0.03	0.02
23 Dev. med. Intensity (0.01 %)	0.42	0.41	0.40	1.30	0.41	0.96
31 Barren (4.97 %)	0.44	0.37	0.12	0.06	0.20	0.43
81 Pasture/hay (0.78 %)	0.51	0.31	0.08	0.36	0.17	0.03
82 Irrigated crops (0.03 %)	1.43	0.62	0.14	0.05	0.19	0.52
2001 Sparse veg. (0.27 %)	0.41	0.51	0.29	0.14	0.53	1.30
2006 Alpine sparse veg. (0.87 %)	0.82	1.56	0.09	0.08	0.21	12.96
2011 Aspen (4.75 %)	0.29	0.23	0.05	0.03	0.12	0.04
2016 Pinyon-juniper (33.96 %)	0.27	0.19	0.11	0.05	0.19	0.07
2051 Dry mixed conifer (1.19 %)	0.23	0.20	0.15	0.04	0.10	0.06
2052 Mixed conifer (0.21 %)	0.53	0.64	0.11	0.07	0.56	0.06
2054 Ponderosa pine woodland (5.48 %)	0.23	0.23	0.15	0.04	0.19	0.04
2055 Dry spruce-fir (1.82 %)	1.73	0.97	0.08	0.03	0.56	12.96
2057 Subalpine limber pine (0.06 %)	12.96	0.18	0.12	0.08	0.95	12.96
2061 Aspen/mixed conifer (1.65 %)	0.66	0.40	0.08	0.05	0.23	0.02
2062 Mtn. mahogany (0.22 %)	0.44	0.28	0.16	0.02	0.11	0.04
2064 Low sagebrush (0.54 %)	0.29	0.23	0.10	0.04	0.17	0.07
2066 Saltbrush scrub (0.04 %)	0.73	0.31	1.10	3.33	0.88	0.51
2080 Big sagebrush (12.82 %)	0.20	0.15	0.15	0.04	0.15	0.06
2081 Salt desert scrub (1.12 %)	0.32	0.21	0.12	0.46	0.19	0.25
2086 Foothill scrub (0.27 %)	0.47	0.36	0.19	0.08	0.11	0.34
2093 Sand shrubland (0.06 %)	0.72	0.64	0.10	5.83	0.70	0.22
2103 Semi-desert chaparral (0.03 %)	0.13	0.31	0.15	0.02	0.18	0.05
2107 Gambel oak (0.05 %)	0.81	0.31	0.09	0.13	12.96	0.08
2117 Ponderosa pine savanna (0.05 %)	0.28	0.33	0.18	0.02	0.23	0.05
2126 Sagebrush steppe (0.33 %)	0.27	0.12	0.08	0.11	0.31	0.03
2135 Semi-desert grassland (0.56 %)	0.28	0.32	0.36	0.61	0.08	0.38
2153 Greasewood flat (0.26 %)	0.33	0.20	0.10	0.65	0.33	0.08
2159 Riparian (2.97 %)	0.29	0.18	0.14	0.04	0.20	0.08
2160 Subalpine riparian (0.31 %)	0.52	0.12	0.07	0.03	0.57	0.08
2180 Intro. riparian (0.81 %)	0.34	0.22	0.19	0.04	0.18	0.12
2181 Annual grass (2.19 %)	0.27	0.17	0.18	0.24	0.13	0.06
2210 Shrubland-blackbrush (14.33 %)	0.26	0.20	0.20	0.11	0.19	0.13
2214 Shrubland-manzanita (0.11 %)	0.28	0.22	0.07	0.05	0.15	0.06
2217 Shrubland-Gambel oak (6.10 %)	0.21	0.20	0.08	0.03	0.08	0.05
2220 Shrubland-big sagebrush (0.21 %)	0.22	0.14	0.20	0.10	0.38	0.03

Percentage of total area is given after each land cover type. Small numbers indicate habitats where deer linger, while large numbers highlight areas they quickly leave

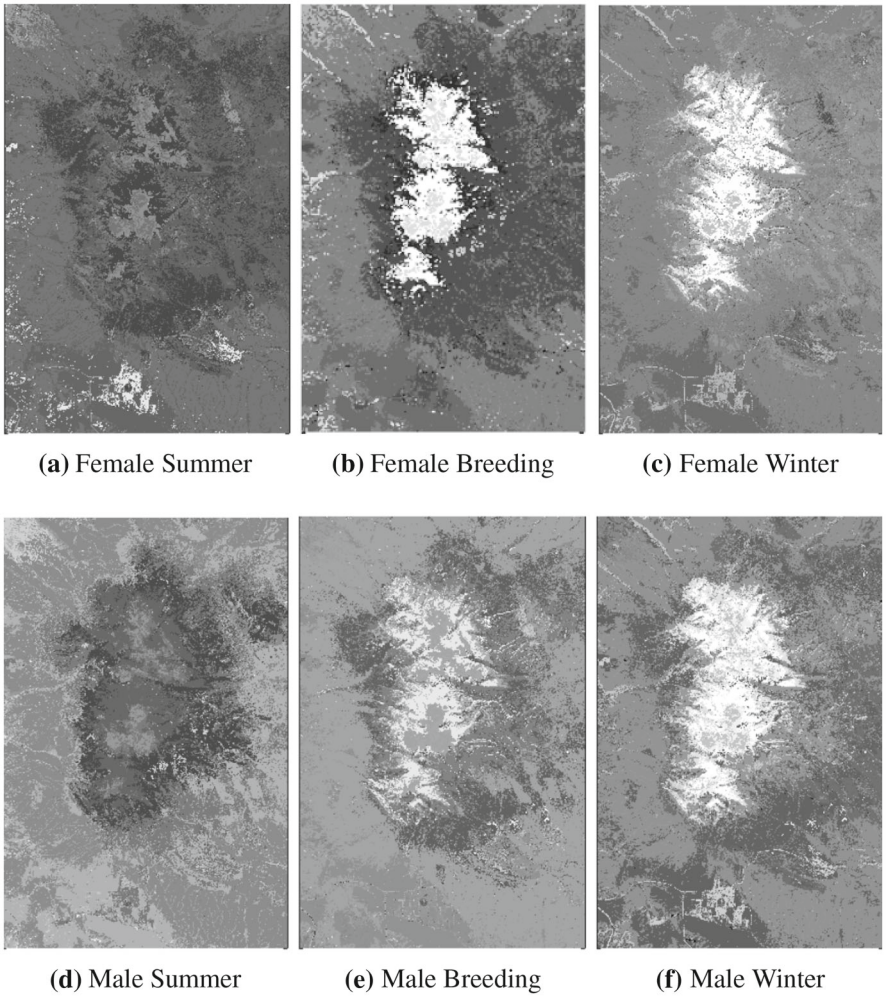

Fig. 3 Comparison of motilities for female and male during summer, breeding season, and winter in an area including the La Sal Mountains. *Dark shades* represent low motility, i.e., areas where the deer aggregate and spend time, while the lighter regions represent high motility i.e., areas that they avoid or move through quickly. In summer the deer are in the mountains and then move to lower elevations for winter

We chose a spatial step of 600 m in both directions and a time step of 5 days although other step sizes work as well. The averaging was done over 3,000 m blocks ($\epsilon = 0.01$). We started with an initial number of infected deer (which depends on the simulation) in the La Sal Mountains and simulated the spread over 10 years. Table 3 displays the results of simulations exploring different infection rates. The number of infected deer were computed from densities (number of infectives per square kilometer) by $N_{IF} = \iint_A I_F dA$ and $N_{IM} = \iint_A I_M dA$, where N_{IF} is the number of infected females and N_{IM} is the number of infected males.

Table 3 Simulations exploring different infection rates for the CWD model over 10 years

Simulation	1	2	3	4	5
Steady-state pop.	22,430 f	22,430 f	22,430 f	22,430 f	22,430 f
	4,070 m	4,070 m	4,070 m	4,070 m	4,070 m
Initial inf.	47 f	47 f	47 f	130 f	47 f
	32 m	32 m	32 m	32 m	32 m
β_{FF}, β_{MF}	8.9315×10^{-5}	5.39×10^{-4}	6.25×10^{-4}	6.25×10^{-4}	6.25×10^{-4}
β_{MM}, β_{FM}	8.9315×10^{-5}	5.39×10^{-4}	6.25×10^{-4}	0.00125	0.00125
Notes	2007 pop.	$\times 6$	$\times 7$	1 % prev. in f	$\beta_{MM} = \beta_{FF} \times 2$
Results					
No. of inf. f	0 f	44 f	199 f	539 f	205 f
No. of inf. m	0 m	1 m	4 m	18 m	7 m
Simulation	6	7	8	9	10
Steady-state pop.	22,430 f	22,430 f	22,430 f	16,957	33,565
	4,070 m	4,070 m	4,070 m	2,543	5,035
Initial inf.	47 f	47 f	47 f	29 f	79 f
	32 m	32 m	32 m	11 m	54 m
β_{FF}, β_{MF}	6.25×10^{-4}	6.25×10^{-4}	7.15×10^{-4}	6.25×10^{-4}	6.25×10^{-4}
β_{MM}, β_{FM}	0.0019	0.0019	0.00212	0.0019	0.0019
Notes	$\beta_{MM} = \beta_{FF} \times 3$	No hazard	$\times 8$	2010 pop.	Obj. pop.
Results					
No. of inf. f	214 f	112 f	1,058 f	7 f	All
No. of inf. m	13 m	5 m	55 m	0 m	All

Steady state-state populations are from population estimations made by the UDWR (2012). Numbers of females are indicated by f and numbers of males by m. The results are in terms of numbers of infected males and females. The simulation numbers (1, 2, . . . , 10) are to aid in referring to particular simulations in the text

The first eight simulations use the 2007 estimated populations (the peak population estimate for the last 10 years) for the study area of 22,430 females and 4,070 males, using an 18:100 buck to doe ratio (from post hunting season population counts). Initial conditions of 2 % prevalence in males (32 infectives) and 0.5 % prevalence in females (47 infectives) were used for Simulations 1–3 and 5–8. The infection rate from Miller et al. (2006) of 8.9315×10^{-5} (Table 3) resulted in the disease dying out in 10 years (Simulation 1). This has not been the case since new cases of CWD have been detected in the La Sal Mountains every year since 2002. Increasing this rate by a factor of ten (i.e. to the nominal value estimated by Miller et al. for penned dear) resulted in all susceptible deer becoming infected. Presumably the 'true' value of the infectivity is in between these two extremes, and we focused other simulations on this regime.

An infection rate of 5.39×10^{-4} ($8.9315 \times 10^{-5} \times 6$) yields one infected male and 44 infected females at the end of 10 years (Simulation 2). Increasing the rate to 6.35×10^{-4} yields 199 infected females and 4 infected males (Simulation 3). Changing the number of initial infected females from 47 to 130 (1 % prevalence) resulted in 539

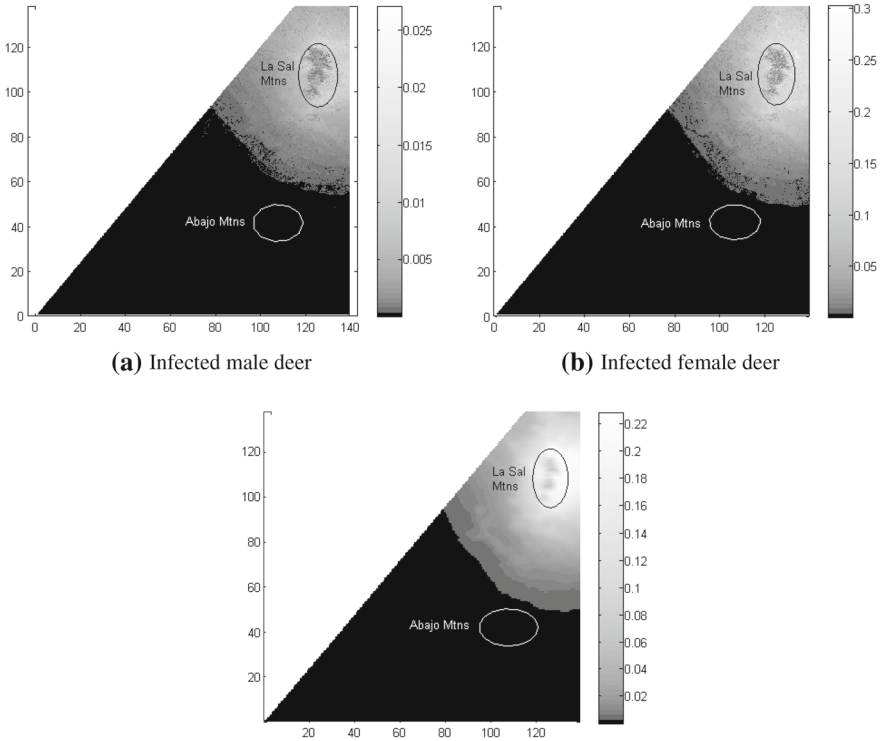

(a) Infected male deer

(b) Infected female deer

(c) Environmental hazard

Fig. 4 The results of running the simulation for 10 years using $\beta_{FF} = \beta_{MF} = 6.5 \times 10^{-4}$ and $\beta_{MM} = \beta FM = 0.0019$. The initial conditions are shown in Table 3, Simulation 6. The *lighter* the *shade* the higher the density (in number per square kilometer) of infected deer in **a** and **b** and the higher the concentration of prions in the environment in **c**. The densities of infected male and female deer were returned to the small scale at the end of the simulations by using interpolation. Environmental hazard, however, remains in terms of the homogenization scale, which accounts for the smooth appearance. The amount of environmental hazard is in units of mass per square kilometer

infected females and 18 infected males (Simulation 4). Arguably male deer engage in risky behaviors (e.g. licking to test for receptivity during breeding season), and potentially should have higher rates of transmission. Returning to 0.5 % prevalence in females and setting the infection rate for males ($\beta_{MM} = \beta_{FM} = 0.00125$) to be twice that of females ($\beta_{FF} = \beta_{MF} = 6.23 \times 10^{-4}$) increases the number of infectives to 205 females and 7 males (Simulation 5). Tripling the infection rate for males gives 214 infected females and 13 infected males (Simulation 6). The result of this simulation is shown in Fig. 4.

Parameters controlling prion release into the environment are the least well established. To see how strongly our model of environmental hazard influences rates of spread we kept the same initial conditions and infection rates but ran the model without prions collecting in the environment (Simulation 7). After 10 years the number of infected females was 112 compared to 214 for the model with environmental

hazard. The number of infected males was 5 compared to 13. Simulation 8 resulted in an increase in infected males (from 32 to 55 over 10 years) by using infection rates $\beta_{FF} = \beta_{MF} = 7.15 \times 10^{-4}$ and $\beta_{MM} = \beta_{FM} = 0.00212$. It is interesting to note that this was the only one of the first eight simulations that resulted in an increase in infected male deer from the initial amount of infectives. The number of infective females, however, increased for lower infection rates. This could be due to the fact that the estimated motilities for males are consistently larger than those for females (see Table 2) in key mule deer habitats, such as sagebrush steppe, pinyon-juniper forest, and ponderosa pine woodland. This means that female deer congregate more, leading to higher rates of transmission, while male deer wander more. This connection between motility and disease spread is a basic feature of the CWD model. Finally, due to harvesting practices, there are about seven times more susceptible females than males (UDWR 2012).

To test model sensitivity to population density we returned to $\beta_{FF} = \beta_{MF} = 6.23 \times 10^{-4}$, $\beta_{MM} = \beta_{FM} = 0.0019$ and varied the steady-state population of susceptibles. The estimated population for the study area for 2010 with 15 bucks to 100 does (from post hunting season population counts) is 16,957 females and 2,543 males. Using these numbers resulted in 7 infected females and 0 infected males (Simulation 9). The goal of the UDWR for the two management units in our study area is to have an objective population of 38,600 mule deer (UDWR 2012). Using this population with the goal of 15 bucks to 100 does, all the deer become infected by the end of 10 years (Simulation 10).

Finally, to illustrate the effects of differential motility, we compared model results with variable motilities to those resulting from constant motility, computed as a weighted average (Simulations 11 and 12 in Table 4). Beginning with 214 infected females and 64 infected males and a susceptible population of 21,348 females and 3,202 males, the model with variable motilities resulted in 890 infected females and 40 infective males after 10 years, compared to 48 infected females and 2 infected males for the mode with constant motility. The spread was much wider for the constant motility model, as expected, but rates of disease transmission were an order of magnitude lower (see Fig. 5). This is a substantial difference, illustrating that low motilities in the variable motility model aggregate deer causing an increase in the number of infectives while slowing the spread into new areas, an effect absent in the constant motility model.

As mentioned at the end of Sect. 2.2, we save computational time by using $\left\langle \frac{H_0}{\mu_F} \right\rangle = \sigma_F \left\langle \frac{1}{\mu_F} \right\rangle \langle H_0 \rangle$ (similar for male motilities). In simulations 13 and 14 (see Table 4) we test this using $\sigma_F = \sigma_M = 1$. The average $\left\langle \frac{H_0}{\mu_F} \right\rangle$ is computed by returning to the small scale every time step. In order to make this computationally feasible, we subsampled the motility matrix for our study area, using every third value. This resulted in 94 infected females and 5 infected males at the end of 10 years. Subsampling in this same manner for the simulation using $\sigma_F \left\langle \frac{1}{\mu_F} \right\rangle \langle H_0 \rangle$, we obtained similar results, 105 infected females and 6 infected males. This indicates that the approximation is worth the computational savings and makes it possible to numerically solve the equations for a large domain.

Table 4 The results of simulations comparing variable motilities with a constant motility (Simulations 11 and 12) and a comparison of two ways of averaging the environmental hazard (Simulations 13 and 14)

Simulation	11	12	13	14
Steady-state pop.	21,348 f	21,348 f	22,430 f	22,430f
	3,202 m	3,202 m	4,070 m	4,070 m
Initial inf.	214 f	214 f	47 f	47 f
	64 m	64 m	32 m	32 m
β_{FF}, β_{MF}	0.0005562	0.0005562	0.000625	0.000625
β_{MM}, β_{FM}	0.0007843	0.0007843	0.0019	0.0019
Notes	2002 pop.	Constant motility	$\left\langle \frac{H}{\mu} \right\rangle$	$\left\langle \frac{1}{\mu} \right\rangle \langle H \rangle$
Results				
No. of inf. f	890 f	48 f	94 f	105 f
No. of inf. m	40 m	2 m	5 m	6 m

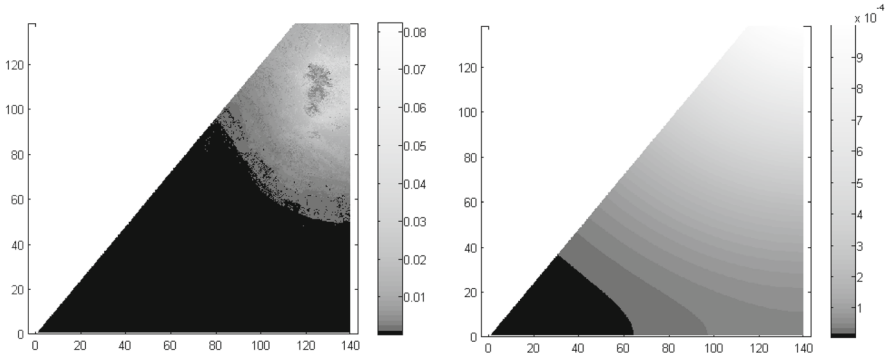

(a) Variable motility coefficient **(b)** Constant motility coefficient

Fig. 5 The density of male infectives simulated with variable motilities (**a**) and with a constant motility (**b**) computed as a weighted average of the male motilities. For the initial vales and infection rates used see Table 4, Simulations 11 and 13. The simulation with variable motilities predicted a total of 930 infected deer after 10 years, while the constant motility simulation predicted a total of 50 infected deer

The motilities for males and females vary with season, so we ran a simulation to compare the spread of CWD over a single season to see if time of year influences spread. The same steady-state susceptible population and number of infectives were used at the beginning of each season. The length of each season is defined by how the GPS movement data was collected (153 days for summer, 61 days for breeding season, and 151 days for winter). The results are found in Table 5 and shown in Fig. 6 for male deer. Even though breeding season is much shorter than winter, the increase in infectives was very similar. However, the spread of infectives during winter was much wider than during breeding season. This may be due to the aggregation of deer on winter ranges increasing the transmission of prions, in concert with the movement that does occur this time of year, as shown by the data. Breeding season had a net increase of 0.23 infected females per day and 0.1 infected males per day, much higher

Table 5 Comparison of CWD spread over one season

Simulation	15	16	17
Steady-state pop.	22,430 f 4,070 m	22,430 f 4,070 m	22,430 f 4,070 m
Initial inf.	47 f	47 f	47 f
	32 m	32 m	32 m
β_{FF}, β_{MF}	0.000625	0.000625	0.000625
β_{MM}, β_{FM}	0.0019	0.0019	0.0019
Notes	1 summer	1 breeding season	1 winter
Results			
No. of inf. f	59 f	61 f	62 f
No. of inf. m	31 m	38 m	40 m
f inf. per day	0.08	0.23	0.1
m inf. per day	−0.007	0.1	0.05

The length of each season is defined by how the GPS movement data was collected (153 days for summer, 61 days for breeding season, and 151 days for winter). The number of infectives per day is the net increase or decrease in the number of infectives divided by the length of the season

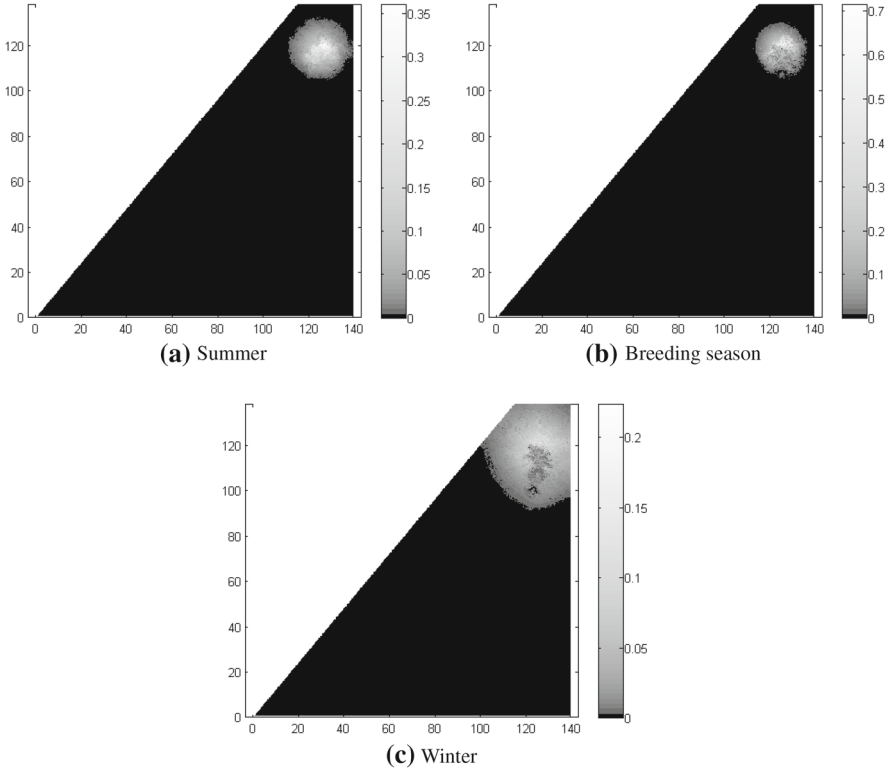

Fig. 6 A comparison of CWD spread for one season for male mule deer. The same initial values were used at the beginning of each season, as found in Table 5. The resulting numbers of infectives were quite similar (31 for summer, 38 for breeding season, and 40 for winter). However, spread occurred over a much larger area during winter than during breeding season and summer

than 0.1 infected females per day and 0.05 infected males per day during winter. This reflects that breeding behaviors can increase the number of new infectives this time of year.

4 Stability and asymptotic speed of spread

As illustrated by the simulations above, use of ecological diffusion, which realistically aggregates populations in favorable environments, and a standard SI disease model allows for habitat to condition how disease spreads. It is easy enough to understand intuitively how this would work; if there is enough favorable habitat to aggregate susceptibles, disease can take off locally. Obviously a critical threshold could be passed if either the susceptible population is large enough or if there are enough small patches of attractive habitat spread amid less favorable environments such that local populations exceed disease outbreak thresholds. However, these mechanisms presuppose landscape variability, and consequently analytically predicting when diseases could invade a landscape seems difficult. Skellam (1951) introduced the idea of biological invasions for constant coefficient reaction–diffusion equations by estimating the speed of the spread of muskrats across Europe. Shigesada and Kawasaki (1997) extended it to ecological diffusion over an environment composed of two types of patches. In this section we will use the results of homogenization to develop a way to calculate invasion speeds over very heterogeneous landscapes, using the averaged coefficients to explore invasion speeds and critical population levels for specific areas.

The spatially-structured "invasibility" of large-scale landscapes can be examined via the homogenized equations (39)–(41). While solutions to the homogenized equations are not the state variables of interest, the infected population is related by rescaling the homogenized solution using the motility (12). Since the motilities are constant within season, disease prevalence can only grow in time if solutions to the homogenized equations grow. Consequently, spread can be investigated by using the homogenized equations, averaging over small-scale variability.

We consider the system without the environmental hazard, assuming that horizontal transmission occurs on a faster time scale than accumulation of prions in the environment. In any event, from the standpoint of invasibility, accumulation of prions would only accelerate transmission, so neglecting prion hazard is a conservative assumption. With this caveat the homogenized system can be written:

$$\partial_t u = D_1 \nabla_x^2 u + A_1 u + A_2 v \tag{45}$$

$$\partial_t v = D_2 \nabla_x^2 v + B_1 v + B_2 u, \tag{46}$$

where $u = c_{IF}$ and $v = c_{IM}$ for notational simplicity. The coefficients, after multiplication by ω to return to the original time scale, are:

$$D_1 = \bar{\mu}_F, \quad D_2 = \bar{\mu}_M \tag{47}$$

$$A_1 = \bar{\mu}_F \left\langle \left(\beta_{FF}\hat{S}_F - \omega - \phi\right) \tfrac{1}{\mu_F} \right\rangle, \quad B_1 = \bar{\mu}_M \left\langle \left(\beta_{MM}\hat{S}_M - \omega - \phi\right) \tfrac{1}{\mu_M} \right\rangle, \tag{48}$$

$$A_2 = \bar{\mu}_F \beta_{MF} \left\langle \tfrac{\hat{S}_F}{\mu_M} \right\rangle, \quad \text{and} \quad B_2 = \bar{\mu}_M \beta_{FM} \left\langle \tfrac{\hat{S}_M}{\mu_F} \right\rangle. \tag{49}$$

At the leading edge of the disease invasion propagating at speed c in the direction (w.l.o.g.) x we assume a traveling solution of the form

$$\begin{pmatrix} u \\ v \end{pmatrix} = \begin{pmatrix} u_0 \\ v_0 \end{pmatrix} e^{\sigma t + \lambda(x - ct)}, \tag{50}$$

where u_0 and v_0 are arbitrary constants, σ is the growth rate, $\lambda < 0$ is the rate of decrease of prevalence in the frame of reference of the front. Substituting (50) into (45) and (46) and rearranging gives the eigenvalue relation,

$$\begin{pmatrix} -\sigma + c\lambda + A_1 + D_1\lambda^2 & A_2 \\ B_2 & -\sigma + c\lambda + B_1 + D_2\lambda^2 \end{pmatrix} \begin{pmatrix} u_0 \\ v_0 \end{pmatrix} = \begin{pmatrix} 0 \\ 0 \end{pmatrix}. \tag{51}$$

Setting the determinant of the matrix in (51) to zero gives the dispersion relation.

Following Okubo et al. (1989), (but using nomenclature as in Powell (1997)), the asymptotic speed can be calculated from the dispersion relation by requiring that $\sigma = 0$ (i.e. the speed is chosen so that there is no growth in the traveling frame of reference) and $\frac{d\sigma}{d\lambda} = 0$ ($\sigma = 0$ is the largest growth rate, so all perturbations to the front will shrink in this frame of reference). These requirements are precisely equivalent to the well-known 'minimum wave speed' approach of Aronson and Weinberger (1978), and result in the system of equations

$$f(c, \lambda, \boldsymbol{\theta}) = (c\lambda + A_1 + D_1\lambda^2)(c\lambda + B_1 + D_2\lambda^2) - A_2B_2 = 0 \tag{52}$$

$$\frac{df}{d\lambda} = (c + 2D_1\lambda)(c\lambda + B_1 + D_2\lambda^2) + (c + 2D_2\lambda)(c\lambda + A_1 + D_1\lambda^2) = 0, \tag{53}$$

where $\boldsymbol{\theta}$ is a vector containing the parameters.

We can obtain an expression for the wave speed, c, by multiplying (52) by -2 and (53) by λ and adding the resulting equations together.

$$c = g(\lambda, \boldsymbol{\theta}) = \frac{-2(D_1D_2\lambda^4 + A_2B_2 - A_1B_1)}{\lambda(D_1\lambda^2 + D_2\lambda^2 - A_1 - B_1)}. \tag{54}$$

We substitute (54) into (52) to obtain a polynomial in λ, $F(\lambda, \boldsymbol{\theta}) = 0$. For a given set of parameters, $\boldsymbol{\theta}$, we can numerically find a point ($\lambda < 0, c$) that satisfies $F(\lambda, \boldsymbol{\theta}) = 0$ and $c = g(\lambda, \boldsymbol{\theta})$.

The parameters, defined in (47)–(49), are dependent on the motilities, μ_F and μ_M, and steady-state population densities, $\hat{S}_F$ and $\hat{S}_M$. The number, N_F, of female deer is given by

$$N_F = \iint_A \hat{S}_F dA = \iint_A \frac{C_F}{\mu_F} dA = C_F A \left\langle \frac{1}{\mu_F} \right\rangle, \tag{55}$$

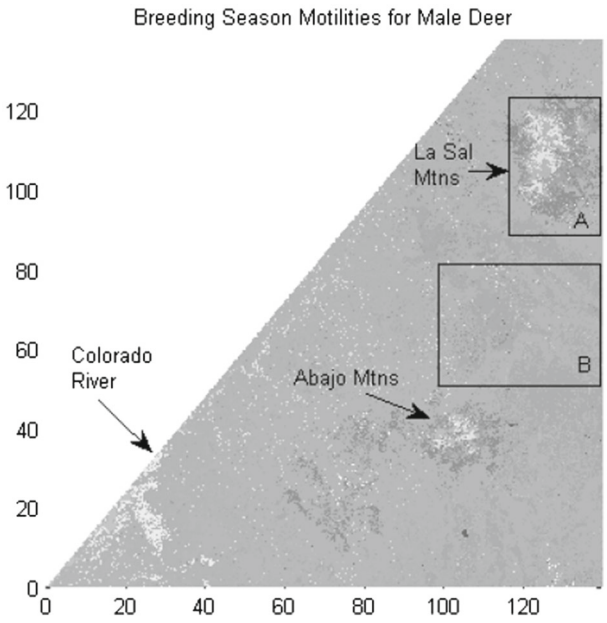

Fig. 7 Areas averaged across for critical population examples. *Area A* includes the La Sal Mountains and is critical summer range for mule deer. It is where CWD was first discovered in Utah (2002). *Area B* is an area between the La Sal and Abajo mountain ranges and is critical winter range

where A is the area of a region of interest. Likewise, the number of males is given by $N_M = C_M A \left\langle \frac{1}{\mu_M} \right\rangle$. Then $C_F = \frac{\mu_F N_F}{A}$ and $C_M = \frac{\mu_M N_M}{A}$ and (48)–(49) become:

$$A_1 = \frac{\bar{\mu}_F^2}{A} \left\langle \frac{1}{\mu_F^2} \right\rangle \beta_{FF} N_F - \bar{\mu}_F \left\langle \frac{1}{\mu_F} \right\rangle (\omega + \phi), \tag{56}$$

$$B_1 = \frac{\bar{\mu}_M^2}{A} \left\langle \frac{1}{\mu_M^2} \right\rangle \beta_{MM} N_M - \bar{\mu}_M \left\langle \frac{1}{\mu_M} \right\rangle (\omega + \phi), \tag{57}$$

$$A_2 = \frac{\bar{\mu}_F^2}{A} \left\langle \frac{1}{\mu_F \mu_M} \right\rangle \beta_{MF} N_F, \quad \text{and} \quad B_2 = \frac{\bar{\mu}_M^2}{A} \left\langle \frac{1}{\mu_F \mu_M} \right\rangle \beta_{FM} N_M. \tag{58}$$

Now our exploration of c values can be framed in terms of N_F and N_M, for an area of interest and given motilities, infection rates, death rate, and cull rate.

To illustrate this, we used two rectangular regions in our study area, shown in Fig. 7. Area A includes the La Sal Mountains and contains critical summer range habitats. It is where CWD was first discovered in Utah in 2002. Area B is critical winter range between the La Sal and Abajo Mountains, and the area through which a wave of infection would have to travel to reach the Abajo Mountains.

Using population estimates for 2007 and 2010, and the population management goal of the UDWR (objective), we calculated the female and male population for each area separately for summer and winter, subject to the respective motilities. Those populations in Area A and Area B for winter are shown as points on the graphs in Fig. 8.

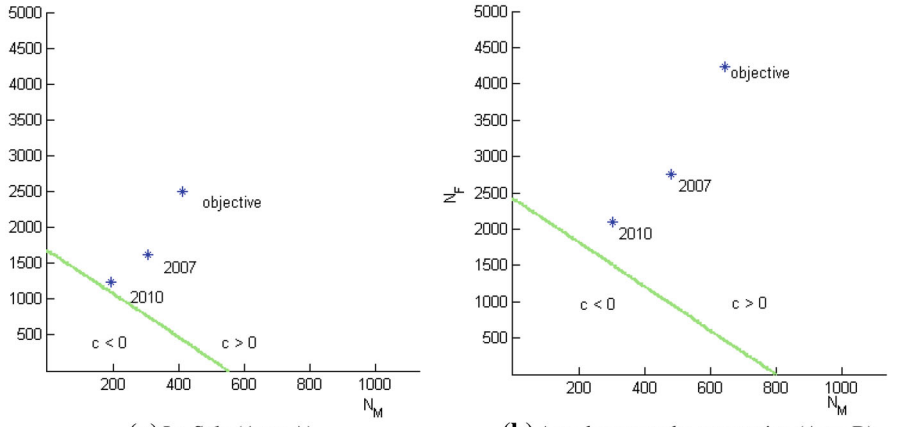

(a) La Sals (Area A) **(b)** Area between the mountains (Area B)

Fig. 8 The *asterisks* show populations for these areas subject to winter motilities for male (N_M) and female (N_F) deer using the population estimates for 2007 and 2010, and the objective goal. The *green curves* indicate where the asymptotic invasive speed is zero using infection rates $\beta_{FF} = \beta_{MF} = 6.23 \times 10^{-4}$ and $\beta_{MM} = \beta_{FM} = 0.0019$. In *Area A* the 2010 estimated population is close to the $c = 0$ *line* (color figure online)

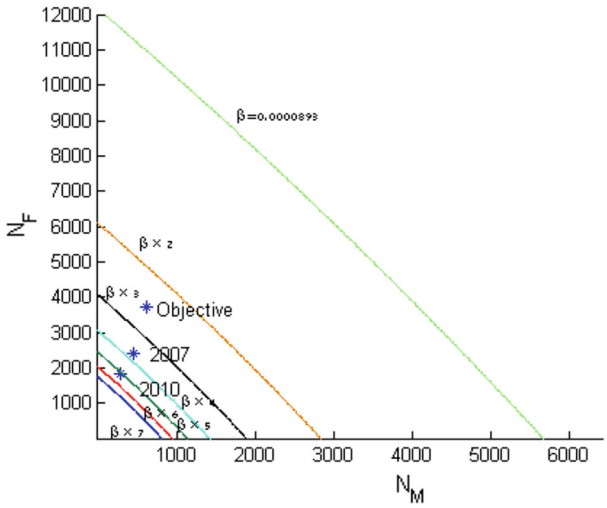

Fig. 9 A comparison of $c = 0$ *lines* for many different infection rates for the La Sals (*Area A*) with summer motilities. The *longest curve* is for an infection rate of $\beta = 8.93 \times 10^{-5}$ as in Miller et al. (2006). This rate is multiplied by 2, then 3, etc. until the curve closest to the origin, which is $\beta = 8.93 \times 10^{-5} = 6.23 \times 10^{-4}$ (the rate used in Fig. 8)

For infection rates $\beta_{FF} = \beta_{MF} = 6.23 \times 10^{-4}$and $\beta_{MM} = \beta_{FM} = 0.0019$, contours of invasion speed, c, are indicated. For these infection rates all of the population points fall in the region of positive invasive speed, although for Area A the 2010 winter population estimate (193 males and 1,233 females) is close to the $c = 0$ curve, indicating a much slower rate of spread.

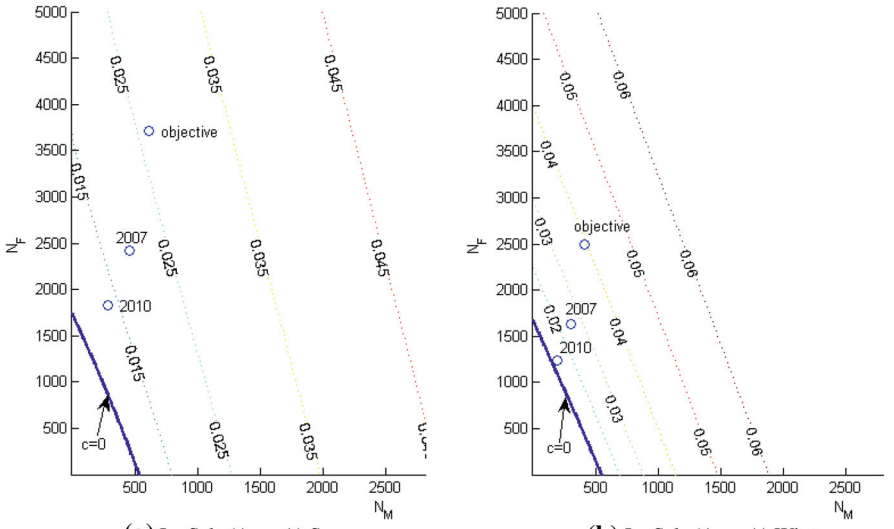

(a) La Sals (Area A) Summer **(b)** La Sals (Area A) Winter

Fig. 10 A look at the contours for speeds, c, *Area A*. With summer motilities the estimated population for 2010 is between $c = 0.01$ and $c = 0.015$ kilometers per day, which is between 3.7 and 5.5 km per year. Using winter motilities, the estimated population for 2010 falls between $c = 0$ and $c = 0.01$, making the speed of invasion for that population less than 3.7 km per year. The infection rates $\beta_{FF} = \beta_{MF} = 6.23 \times 10^{-4}$ and $\beta_{MM} = \beta_{FM} = 0.0019$ were used

Figure 9 compares the $c = 0$ curves for a variety of infection rates for Area A with summer motilities. The scaled infection rate from Miller et al. (2006), 8.93×10^{-5}, produces a threshold at the highest population values. This rate would mean that the disease for all the population estimates would not diffuse from the La Sals under current population levels (as indicated in simulation 1 above). The discovery of CWD in the Abajos indicates that the disease has spread from the La Sals. An infection rate of greater than 3.57×10^{-4} is needed for spread from a population the size of the 2007 estimate. This increases to 5.36×10^{-4} for a population at the 2010 level.

Figure 10 includes contours of speed, c, for Area A, comparing summer and winter results, using $\beta_{FF} = \beta_{MF} = 6.23 \times 10^{-4}$ and $\beta_{MM} = \beta_{FM} = 0.0019$. The units of c are kilometers per day. Converting them to kilometers per year helps put population size into the context of the speed needed for CWD to spread the 100 kilometers from the La Sal Mountains to the Abajo Mountains. For summer (Fig. 10a) $9.125 < c < 10.95$ km year^{-1} at the objective population level, while $c < 5.475$ km year^{-1} at the 2010 population level. For winter the 2007 population level c is between 7.3 km year^{-1} and 10.95 km year^{-1}. This would be a rate fast enough for the disease to spread 100 kilometers from the La Sals to the Abajos in approximately 10 years.

5 Discussion and conclusion

In this paper we have presented a spatial model for the spread of CWD in Utah, incorporating ecological diffusion as a way to connect disease spread to animal movement.

Ecological diffusion, in contrast to the more commonly used Fickian diffusion, allows populations to aggregate in desirable regions and avoid undesirable habitat. Consequently, differential motility in landscapes affects both animal movement and the density-dependent transmission of disease. Motility coefficients were estimated separately for each season for both male and female deer, and incorporated into a sex-structured SI model for disease transmission. Homogenization techniques allowed us to model spread of CWD over a large area with computational ease and analyze asymptotic rates of spread in heterogenous landscapes. CWD has been present in the La Sal Mountains for 10 years and has just recently been detected in the Abajos. Our simulations showed that this time line is plausible for infection rates similar to those estimated by Miller et al.

Connecting the landscape with speed of invasion and critical population levels can be important from a management perspective. The permeability of key portions of the landscape for different population levels and infectivities can be analyzed using the methods of Sect. 4. These methods allow spread to be analyzed separately for areas of high and low disease prevalence, land use, and recreational impact, which opens up the possibility of managing populations to stop disease spread into critical areas. Current populations increase spread, but lower target populations in selected areas could potentially stop spread from those areas; our methods provide a way to estimate critical population sizes for differing landscapes.

In the future this model could be applied to other areas in the Western U.S. where CWD is a concern to wildlife managers. Also, the techniques outlined can be extended to many ecological applications. Not only can they be used to model other wildlife diseases, but they can be applied to insect infestations, invasive species, and escaped genetically modified organisms. Tying the spatial structure of the environment to how organisms move is key to understanding spread and invasive speed of organisms and diseases. This is not a new revelation, however, the computational and analytic costs of implementing rational movement models in complex landscapes has prohibited their development. With the use of homogenization in models for ecological diffusion, we have removed barriers to incorporating variable landscapes and discontinuous movement in ecologically meaningful models.

Acknowledgments This research was partially funded by USGS 1434-06HQRU1555. We would like to thank the Utah Division of Wildlife Resources for providing telemetry data and Ben Crabb for providing landcover data. Any use of trade names is for descriptive purpose only and does not imply endorsement by the U.S. Government.

References

Almberg ES, Cross PC, Johnson CJ, Helsey DM (2011) Modeling routes of chronic wasting disease transmission: environmental prion persistence promotes deer popoulation decline and extinction. PLoS ONE 6:e19,896

Anderson RM, May RM (1979) Population biology of infectious diseases. Part 1. Nature 280:361–367

Aronson DG, Weinberger HF (1978) Multidimensional nonlinear diffusion arising in populaiton dynamics. Adv Math 30:33–76

Baeten LA, Powers BE, Jewell JE, Spraker TR, Miller MW (2007) A natural case of chronic wasting disease in a free-ranging moose (Alces alces shirasi). J Wildl Dis 43:309–314

Bar-David S, Lloyd-Smith JO, Getz WM (2006) Dynamics and management of infectious disease in colonizing populations. Ecology 87:1215–1224

Conner MM, Miller MW (2004) Movement patterns and spatial epidemiology of a prion disease in mule deer popoulation units. Ecol Appl 14:1870–1881
Department of Interior GS (2006) The national map LANDFIRE: LANDFIRE national existing vegetation type layer. http://gisdata.usgs.net/website/landfire/
Dewhirst S, Lutscher F (2009) Dispersal in heterogeneous habitats: Thresholds, spatial scales, and approximate rates of spread. Ecology 90:1338–1345
Farnsworth ML, Wolfe LL, Hobbs NT, Burnham KP, Williams ES, Theobald DM, Conner MM, Miller MW (2005) Human land use influences chronic wasting disease prevalence in mule deer. Ecol Appl 15:119–126
Farnsworth ML, Hoeting JA, Hobbs NT, Miller MW (2006) Linking chronic wasting disease to mule deer movement scales: A hierarchical Bayesian approach. Ecol Appl 16:1026–1036
Fitzgibbon WE, Langlais M, Morgan JJ (2001) A mathematical model of the spread of feline leukemia virus (felv) through a highly heterogeneous spatial domain. SIAM J Math Anal 33:570–588
Garlick MJ (2012) Homogenization of large-scale movement models in ecology with application to the spread of chronic wasting disease in mule deer, PhD thesis. Utah State University, Utah
Garlick MJ, Powell JA, Hooten MB, McFarlane LR (2011) Homogenization of large-scale movement models in ecology. Bull Math Biol 73:2088–2108
Gross JE, Miller MW (2001) Chronic wasting disease in mule deer: Disease dynamics and control. J Wildl Manag 65:205–215
Hanks EM, Hooten MB, McFarlane LR, Mock KE (2010) Model-based approaches for characterizing spatial genetic flow. In: JSM proceedings, biometrics section. American Statistical Association
Holmes EE, Lewis MA, Banks JE, Veit RR (1994) Partial differential equations in ecology: spatial interactions and population dynamics. Ecology 75:17–29
Holmes MH (1995) Introduction to perturbation methods. Springer, New York
Hosseini PR, Dhondt AA, Dobson AP (2006) Spatial spread of an emerging infectious disease: conjunctivitis in house finches. Ecology 87:3037–3046
Johns CJ, Mehl CH (2006) A dynamic spatial model for chronic wasting disease in Colorado. J Data Sci 4:21–37
Johnson CJ, Pederson JA, Chappell RJ, McKenzie D, Aiken JM (2006) Oral transmissibility of prion disease is enhanced by binding to soil particles. Public Libr Sci Pathog 3:874–881
Johnson DS, London JM, Lea MA, Durban JW (2008) Continuous-time correlated random walk model for animal telemetry data. Ecology 89:1208–1215
Joly DO, Samuel MD, Langenberg JA, Blanchong JA, Batha CA, Rolley RE, Keane DP, Ribic CA (2006) Spatial epidemiology of chronic wasting disease in Wisconsin white-tailed deer. J Wildl Dis 42:578–588
Kallen A, Arcuri P, Murray JD (1985) A simple model for the spatial spread and control of rabies among foxes. J Theor Biol 116:377–393
Kendall DG (1965) Mathematical models of the spread of infection. Medical Research Council, HMSO, London
Krumm CE, Connor MM, Miller MW (2005) Relative vulnerability of chronic wasting disease infected mule deer to vehicle collisions. J Wildl Dis 41:503–511
Kucera TE (1978) Social behavior and breeding system of the desert mule deer. J Mammal 59:463–476
McFarlane LR (2007) Breeding behavior and space use of male and female mule deer: an examination of potential risk differences for chronic wasting disease infection, Master's thesis. Utah State University, Utah
Miller MW, Wild MA (2004) Epidemiology of chronic wasting disease in captive white-tailed and mule deer. J Wildl Dis 40:320–327
Miller MW, Williams ES (2003) Prion disease: Horizontal prion transmission in mule deer. Nature 425:35–36
Miller MW, Williams ES, McCarty CW, Spraker TR, Kreeger TJ, Larsen CT, Thorne ET (2000) Epizootiology of chronic wasting disease in free-ranging cervids in Colorado and Wyoming. J Wildl Dis 36:676–690
Miller MW, Williams ES, Hobbs NT, Wolfe LL (2004) Environmental sources of prion transmission in mule deer. Emerg Infect Dis 10:1003–1006
Miller MW, Hobbs NT, Tavener SJ (2006) Dynamics of prion disease transmission in mule deer. Ecol Appl 16:2208–2214
Miller MW, Swanson HM, Wolfe L, Quartarone FG, Huwer SL, Southwick CH, Lukacs PM (2008) Lions, prions and deer demise. Public Libr Sci ONE 3:1–7

Mitchell AR, Griffiths DF (1980) The finite difference method in partial differential equations. Wiley, New York
Murray JD, Stanley EA, Brown DL (1986) On the spatial spread of rabies among foxes. Proc R Soc Lond B 229:111–150
Nicholson MC, Bowyer RT, Kie JG (1997) Habitat selection and survival of mule deer: tradeoffs associated with migration. J Mammal 78:483–504
Okubo A, Levin SA (2001) Diffusion and ecological problems: modern perspective interdisciplinary applied mathematics. Springer, New York
Okubo A, Maini PK, Williamson MH, Murray JD (1989) On the spatial spread of the grey squirrel in Britain. Proc R Soc Lond Ser B 238:113–125
Ostfeld RS, Glass GE, Keesing F (2005) Spatial epidemiology: an emerging (or re-emerging) discipline. Trends Ecol Evol 20:328–336
Ovaskainen O (2008) Analytical and numerical tools for diffusion-based movement models. Theor Popul Biol 73:198–211
Pech RP, McIlroy JC (1990) A model of the velocity of advamce of foot and mouth disease in feral pigs. J Appl Ecol 27:635–650
Plummer AP, Christensen DR, Monsen SB (1968) Restoring big-game range in Utah, Tech. rep. Utah Division of Fish and Game, Utah
Powell JA (1997) Conditional stability of front solutions. J Math Biol 35:729–747
Powell JA, Zimmermann NE (2004) Multiscale analysis of active seed dispersal contributes to resolving Reid's paradox. Ecology 85:490–506
Rasmussen R (2012) Southeast utah. http://raysweb.net
Real LA, Biek R (2007) Spatial dynamics and genetics of infectious diseases on heterogeneous landscapes. J R Soc Interface 4:935–948
Schauber EM, Woolf A (2003) Chronic wasting disease in deer and elk: a critique of current models and their application. Wildl Soc Bull 31:610–616
Shigesada N, Kawasaki K (1997) Biological invasions: theory and practice. Oxford University Press, Tokyo
Skellam JG (1951) Random dispersal in theoretical populations. Biometrika 38:196–218
Smith DL, Lucey B, Waller LA, Childs JE, Real LA (2002) Predicting the spatial dynamics of rabies epidemics on heterogeneous landscapes. Proc Natl Acad Sci USA 99:3368–3672
Turchin P (1998) Quantitative analysis of movement. Sinauer Associates, Inc. Publishers, Sunderland
UDWR (2012) Utah division of wildlife resources: chronic wasting disease in Utah. http://wildlife.utah.gov
Watkins BE, Bishop CJ, Bergman EJ, Bronson A, Hale B, Wakeling BF, Carpenter LH, Lutz DW (2007) Habitat guidelines for mule deer: Colorado plateau shrubland and forest ecoregion, Tech. rep. Mule Deer Working Group, Western Association of Fish and Wildlife Agencies
Wild MA, Hobbs NT, Graham MS, Miller MW (2011) The role of predation in disease control: a comparison of selective and nonselective removal on prion disease dynamics in deer. J Wildl Dis 47:78–93
Williams ES (2005) Chronic wasting disease. Vet Pathol 42:530–549